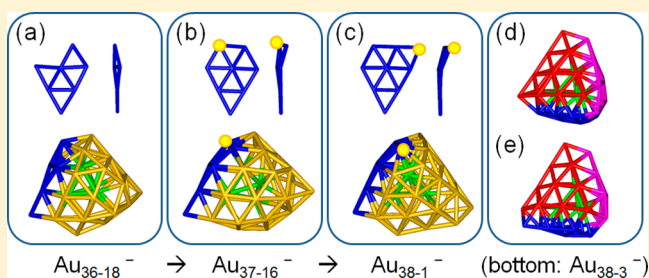


Structural Evolution of Medium-Sized Gold Clusters Au_n^- ($n = 36, 37, 38$): Appearance of Bulk-Like Face Centered Cubic Fragment

Nan Shao,[†] Wei Huang,[‡] Wai-Ning Mei,[†] Lai Sheng Wang,^{*,§} Qin Wu,^{*,||} and Xiao Cheng Zeng^{*,⊥}[†]Physics Department, University of Nebraska–Omaha, Omaha, Nebraska 68182, United States[‡]School of Environmental Science & Optoelectronic Technology, University of Science and Technology of China, Hefei, Anhui 230026, China[§]Chemistry Department, Brown University, Providence, Rhode Island 02912, United States^{||}Center for Functional Nanomaterials, Brookhaven National Laboratory, Upton, New York 11973, United States[⊥]Chemistry Department, University of Nebraska–Lincoln, Lincoln, Nebraska 68588, United States

S Supporting Information

ABSTRACT: We report a joint experimental and theoretical study of the structural evolution of medium-sized gold clusters. We find that the most stable structures of Au_{36}^- to Au_{38}^- exhibit core–shell type structures all with a highly robust tetrahedral four-atom core. All three clusters are observed to possess two coexisting isomers in the cluster beam. The appearance of a fragment of the face centered cubic (FCC) bulk gold, that is, the pyramidal Au_{20}^- , at the size of Au_{38}^- implies that the cluster-to-bulk transformation starts to emerge at the medium size range. It is expected that larger pyramidal-like intermediates may emerge in later medium- to large-sized Au clusters beyond Au_{38}^- .



I. INTRODUCTION

Gold is one of the most noble metals in the periodic table. The fascinating properties of gold include not just its unfading color, but also its high catalytic activities at the nanoscale sizes, stemming from strong relativistic effects.^{1,2} For example, bare or supported Au nanoclusters have been widely reported to be capable of catalyzing the oxidation of CO to CO₂ at low temperatures.^{3–6} Although the understanding of the reaction mechanisms is still incomplete, one important factor for the high activity of supported Au clusters is the propensity of charge transferring between the molecular adsorbates and gold,^{7–9} which is closely related to the size, geometry, and charge of the gold clusters. In addition, low-coordinated sites on the surface of small gold clusters are capable of adsorbing oxygen molecules and more likely to be the active sites.^{10,11} The triangular Au₃ sites on pyramidal Au clusters were recently predicted to be highly active for the CO-self-promoted oxidation.¹² Gaining such mechanistic insights starts with precisely determining the structures of gold clusters.

Although the study of novel properties of Au clusters has achieved a great deal of success through many joint theoretical and experimental efforts over the past two decades, structural determination of gold clusters still proceeds slowly due to strong relativistic and spin–orbit effects of Au, as well as the large number of possible isomers with increasing cluster size. Today, precise global-minimum structures of many small to medium-sized Au clusters have been determined via combining theoretical global-minimum searches with experimental studies,

either by trapped-ion electron diffraction (TIED)^{13,14} or by size-selected photoelectron spectroscopy (PES).^{15,16} For example, it has been found that for anion gold clusters, the two-dimensional (2D) to three-dimensional (3D) structural transition occurs at Au_{12}^- .¹⁷ The hollow-cage structures emerge in the size range of Au_{16}^- – Au_{18}^- .^{16b} The magic number Au_{20}^- cluster has a highly stable tetrahedral pyramid structure, which can be viewed as a fragment of the face centered cubic (FCC) lattice of bulk gold.^{16a} Au_{25}^- was predicted to be the smallest core–shell cluster with a single-atom core.¹⁸ Beyond Au_{25}^- , the low-symmetry core–shell structures dominate the low-energy clusters, and the hollow-cage structures are unlikely to exist in larger size due to the strong relativistic effects.¹⁹

In a previous joint density-functional theory (DFT) and PES experimental study, we found that the core of Au clusters grows gradually from one atom in Au_{25}^- to a tetrahedral four-atom core at Au_{34}^- .^{19–22a} The core-shell structures have been confirmed in other studies.^{22–24} Besides the core growth, the structural evolution of the shell is also traceable. Au_{34}^- was found to be a highly stable cluster and could be viewed as adding an Au atom to the surface of Au_{33}^- to form a more round and robust structure. Au_{35}^- in turn can be viewed as adding one more atom on the surface of Au_{34}^- to start a new shell.¹⁹ Moreover, the core–shell growth was also observed in

Received: January 17, 2014

Revised: February 25, 2014

Published: February 26, 2014

larger clusters. Au_{58}^- was found early to be a highly stable and nearly spherical cluster, and a new shell started at Au_{59}^- and grew to Au_{64}^- in an atom-by-atom fashion.²³ Jiang and Walter suggested that the tetrahedral Au_4 core, which started in Au_{33}^- ,¹⁹ is highly stable in medium-sized Au clusters. As such, they proposed a twisted pyramidal Au_{40} with the tetrahedral core and found it has a relatively large HOMO–LUMO (H–L) gap (0.69 eV) using DFT calculation.^{22b} In a more recent theoretical study of Au_{38}^- , Luo and coworkers also suggest a spindle-like structure of Au_{38}^- , which contains a tetrahedral core.²⁴

The structures of gold clusters in the size regime between 36 and 54 atoms have not been confirmed experimentally. In search for such structural information, the questions are: Is the tetrahedral core so stable that it can be retained in Au clusters beyond the size Au_{36}^- ? If it is, at what size of Au cluster would the tetrahedral core transform to a different core? Also, what would the next core structure look like? To answer some of these questions and to understand the structural growth pattern of medium-sized Au clusters, we have performed a global structure search of low-energy clusters of Au_{36}^- to Au_{38}^- by using the basin-hopping (BH) global optimization method²⁵ combined with DFT calculations. The most stable structures are identified by comparing the experimental PES spectra with the computed electronic density of states of all lowest-lying isomers.^{16,26} We then analyze these structures in detail and suggest possible growth patterns in these clusters.

II. EXPERIMENTAL AND THEORETICAL METHODS

In the PES experiment, the Au clusters were generated from a laser vaporization supersonic cluster source coupled with a time-of-flight mass spectrometer for cluster size selection.²⁷ The clusters of interest were mass-selected and decelerated before photodetachment by a 193 nm (6.424 eV) laser beam from an ArF excimer laser. The photoemitted electrons were collected by a magnetic-bottle and analyzed in a 3.5 m long electron time-of-flight tube. The apparatus was calibrated by the known spectrum of Au^- , and the resolution of the apparatus was $\Delta E_k/E_k \approx 2.5\%$. For more details of the experiments, also see reference 28.

For the theoretical study, we employed the basin-hopping (BH) global optimization method coupled with DFT geometric optimization to generate typically ~ 200 low-energy local-minimum isomers for Au_{36}^- to Au_{38}^- each. The gradient corrected Perdew–Burke–Ernzerhof (PBE) exchange–correlation functional²⁹ and the double numerical polarized (DNP) basis set with effective core potentials (ECPs), implemented in the DMol³ 4.0 code^{30,31} were used for the geometric optimization after each BH step. The top 100 isomers generated were reranked and selected through reoptimization at the fine level of PBE/DND/ECP. The criteria for the selection of low-lying candidates at PBE/DND/ECP (fine) level are 2-fold: the relative energy with respect to the lowest-lying isomer is less than 0.4 eV; and the calculated energy gap between the first and the second major peaks (which, for even number of atoms, is also the H–L gap of the neutral cluster) is within the limit of the experimental energy gap between the first and the second vertical detachment energies (VDEs) $\Delta E_{\text{exp}} \pm 0.04$ eV. Prior to the simulation of PES spectra, the top 10–20 candidate isomers were reoptimized using the hybrid PBE (PBE0) functional and triple- ζ plus polarization (TZP) basis set with the scalar relativistic effect accounted through the zero-order-regular approach (ZORA) implemented in the ADF

code.³² In previous studies, we found that it is important to include the spin–orbit (SO) effect in the calculation of the electronic density of states to achieve the best agreement between theoretical and experimental PES spectra.¹⁹ Here, we computed the PES spectra of all top 10–20 candidate isomers at the SO-PBE0/CRENBL/ECP level, implemented in the NWCHEM 6.0 code.³³ Although we have only studied charged clusters for comparison of PES experiments, we expect the charge effect to be small for medium-sized clusters because this charge is shared by all gold atoms, leading to an insignificant amount of charge per atom.

III. RESULTS

Electronic properties of all candidate isomers are presented in Table 1, and the simulated PES spectra are compared with the experimental spectra in Figures 1–3. We will discuss each cluster in detail in the next section. In Table 1, the first column is the number of core atoms, with mostly four-atom cores and a few three-atom cores. The second column is the original energy orders of isomers (during BH search) at PBE/DND/ECP (fine) level, and these orders are used to label each candidate isomer. The third column is the relative electronic energies of the candidate isomers with respect to the lowest-energy isomer computed at the PBE/DND/ECP (fine) level. From the fourth to sixth column, the results are obtained at the SO-PBE0/CRENBL/ECP//PBE0/TZP(ZORA) level. Relative energies obtained by SO-PBE0/CRENBL/ECP have nearly the same trend as those at PBE/DND/ECP (fine) level with only a few tenths electronvolt in difference. The first vertical-detachment energy (VDE) of each candidate isomer is computed as the energy difference between the neutral and anion cluster based on the optimized anion structure. Note that with the inclusion of the SO effects, computed VDEs in Table 1 are systematically shifted to be lower by ~ 0.1 to 0.3 eV as compared to experimental VDEs.¹⁹ To make the comparison with experimental PES spectra clearer, we align the first VDE of simulated spectra with the experimental spectra (see Figures 1–3). Structures of all candidate isomers are plotted in the Supporting Information (Figure S1). The top candidates that give the best agreement with the experiments are highlighted in bold in Table 1.

IV. DISCUSSION

Au_{36}^- . The experimental spectrum of Au_{36}^- is shown in Figure 1, exhibiting eleven well-separated major peaks for binding energies < 5.5 eV. The discrete peaks below 5.5 eV are mainly the gold 6s band region, and this energy region usually gives characteristic spectral features, which are used to compare with the simulated spectra. The X', A' and B' denote contributions of minor low-lying isomers in the experiment. The top-candidate isomer Au_{36-18}^- exhibits D_2 symmetry and a tetrahedral core, and the eight peaks of the simulated spectrum of Au_{36-18}^- match the corresponding eight peaks of the experimental spectrum very well. This isomer also has the second lowest energy at the DFT level of theory in anion state among low-lying candidates shown in Table 1. The energy gap of 0.36 eV between the first and second major peaks is also the H–L gap of Au_{36-18}^- . The calculated VDE is 0.29 eV less than the experimental VDE. As compared to the reported structure of Au_{35a}^- ,¹⁹ we find that Au_{36-18}^- can be viewed as adding one Au atom on the surface of the best isomer Au_{35a}^- , resulting in two sharp vertexes on the surface of Au_{34}^- (Au_{35a}^- exhibits one

Table 1. Electronic Properties of Top Candidates of Au_{36}^- to Au_{38}^-

N/C	no. ^a	$\Delta E_{\text{PBE/DND}}^a$	ΔE^b	energy gap ^b	VDE ^{b,c}
4	11	0.00	0.00	0.60	3.43
4	18	0.04	0.18	0.36	3.35 (+0.29)
4	29	0.12	0.24	0.31	3.41
4	35	0.15	0.29	0.29	3.39
4	38	0.18	0.29	0.31	3.41
4	44	0.21	0.30	0.38	3.47
4	46	0.22	0.42	0.43	3.54
4	50	0.23	0.47	0.75	3.28 (+0.18)
3	51	0.23	0.49	0.39	3.64
4	53	0.25	0.53	0.32	3.50
4	56	0.26	0.38	0.36	3.51
4	64	0.30	0.49	0.30	3.41
4	83	0.42	0.61	0.30	3.48

Exp. Gap: 0.36 eV (XA)/0.77 eV (X'A'); Exp. VDE: 3.64 (X)/3.46 eV (X')

4	1	0.00	0.00	0.15	3.87
3	3	0.18	0.43	0.24	4.05
4	8	0.22	0.40	0.13	3.98
4	9	0.25	0.30	0.13	4.04 (+0.15)
4	14	0.31	0.41	0.09	3.77
3	15	0.31	0.71	0.18	3.98
4	16	0.32	0.47	0.27	3.66 (+0.15)
4	19	0.32	0.52	0.11	4.13
3	38	0.43	0.79	0.19	3.86
3	44	0.47	0.74	0.18	3.98
4	46	0.48	0.59	0.34	3.80
4	48	0.48	0.63	0.25	3.87
4	51	0.51	0.64	0.19	3.96
4	52	0.51	0.62	0.13	3.98
3	61	0.56	1.06	0.20	3.83

Exp. Gap: 0.23 eV (XA)/0.10 eV (X'A'); Exp VDE: 3.82(X)/4.17 eV (X')

4	1	0.00	0.06	0.35	3.66 (+0.15)
4	2	0.02	0.09	0.38	3.71
4	3	0.04	0.07	0.44	3.59 (+0.15)
4	5	0.16	0.14	0.47	3.55
4	9	0.21	0.00	0.29	3.66
4	15	0.33	0.46	0.35	3.55
4	17	0.36	0.45	0.37	3.63
4	20	0.36	0.43	0.42	3.57

Exp. Gap: 0.34 eV(XA)/0.44 eV(X'A'); Exp VDE: 3.72(X)/3.83 eV(X')

^aComputed at PBE/DNP/ECP(fine) level. ^bComputed at SO-PBE0/CRENBL/ECP//PBE/TZP(ZORA) level. ^cNumbers in parentheses are the shifts needed for aligning first VDE with experiments.

sharp vertex on the surface). Au_{36-50}^- has been assigned as the minor isomer, which has a large H–L gap of 0.75 eV and one vertex on the surface. The electronic density of states of Au_{36-50}^- is plotted at one-half the height of Au_{36-18}^- for clarity in Figure 1.

Au_{37}^- . On the basis of the experimental PES spectrum of Au_{37}^- shown in Figure 2, the first peak X corresponds to one detachment channel and is also much lower in intensity than the next three sharp peaks, indicating the coexistence of major isomers with quite different first VDE. One major isomer is supposed to have 3.82 eV first VDE and 0.23 eV energy gap between the first and second peaks, and the other should fit the rest of the spectrum. In addition, a similar but a slightly smaller energy gap than Au_{36}^- between the binding energy 4.0 and 4.7

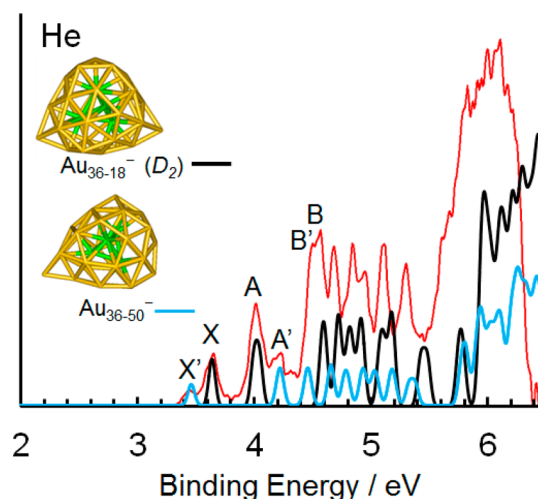


Figure 1. Comparison of experimental and theoretical photoelectron spectra of Au_{36}^- . Red line is the experimental spectrum. Core atoms are highlighted in green.

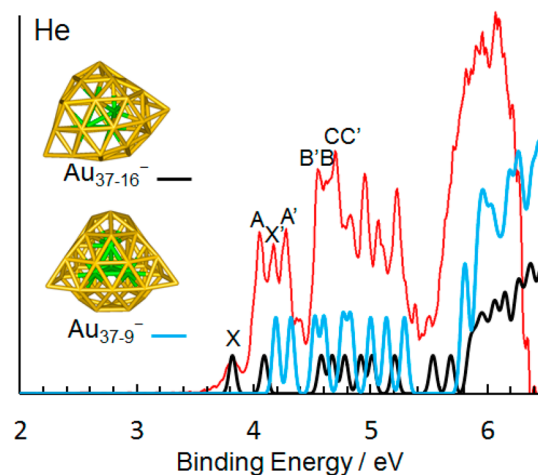


Figure 2. Comparison of experimental and theoretical photoelectron spectra of Au_{37}^- .

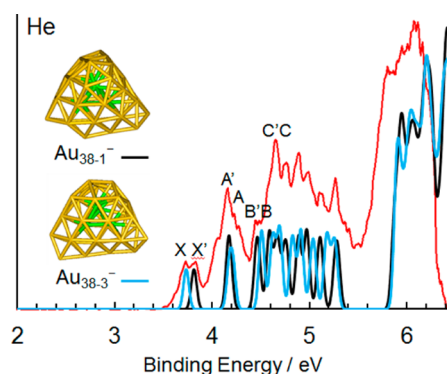


Figure 3. Comparison of experimental and theoretical photoelectron spectra of Au_{38}^- .

eV is also a main feature in the experimental spectrum. In Table 1, Au_{37-1}^- (with C_s symmetry) has much lower energy than all other candidate isomers. However, because including Au_{37-1}^- would require three isomers to fit the experimental spectrum (see Supporting Information Figure S2), it is excluded from being a candidate of major isomers. In this case, additional

isomers with a larger relative energy (0.6 eV) with respect to Au_{37-1}^- are included as candidate isomers (see Table 1). We first assign the Au_{37-16}^- (with C_1 symmetry) as one of the two major isomers. The first and second major peaks of its PES spectrum are in good agreement with the experimental ones, as are the later peaks between 4.5 and 5.3 eV. The extremely low VDE of Au_{37-16}^- (3.66 eV) confirms its contribution to the first VDE peak in the experimental PES spectrum. We also notice that the computed spectrum of Au_{37-16}^- is similar to that of Au_{36-18}^- . In Figures 1 and 2, both spectra exhibit eight major peaks before 5.5 eV. The unpaired electron of Au_{36-18}^- gets paired up in the Au_{37-16}^- . The similarity in their spectra indicates both clusters possess nearly the same structure. Besides Au_{37-16}^- , Au_{37-9}^- (with C_s symmetry) is assigned as the second major isomer of Au_{37}^- . The electronic density of states of Au_{37-16}^- is plotted at one-half the height of Au_{37-9}^- for clarity. In Figure 2, peaks X to A' are fitted by Au_{37-16}^- and Au_{37-9}^- very well. The peaks between 4.5 and 5.3 eV are difficult to compare with the simulated spectra due to the mix of two major isomers.

Au_{38}^- . The experimental spectrum of Au_{38}^- (Figure 3) also indicates coexistence of two major isomers in the cluster beam. As an open-shell cluster, Au_{38}^- should exhibit a relatively lower first peak in its PES spectrum corresponding to the unpaired electron added to Au_{38} . The slightly separated peaks X and X' (Figure 3) with the same low relative intensities, the intense and broad peak A, as well as the dense congested features between 4.5 and 5.3 eV all support that the two major isomers are likely to have similar structures. We assign Au_{38-1}^- and Au_{38-3}^- as the two coexisting isomers of Au_{38}^- , with the H–L gap being 0.35 and 0.44 eV, respectively. Also, due to the mix of two isomers, we can only assign peaks B', B, C', and C to the two isomers. Interestingly, both Au_{38-1}^- and Au_{38-3}^- exhibit some close-packed FCC character in their structures, which will be discussed in the following section.

Structural Evolution and Growth Pattern. All of the isomers found for Au_{36}^- to Au_{38}^- have the core–shell type structures. We can gain some insights into the shape and structural features of these clusters through the atom-to-center distance distribution (see Figure 4). In Figure 4, each peak was

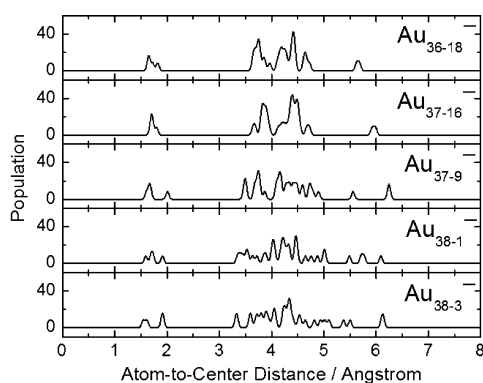


Figure 4. Atom-to-center distance distributions for top candidate isomers of Au_{36}^- to Au_{38}^- .

fitted with a Gaussian of width 0.05 Å to give the population of distance. One generic structural feature is that all top candidate isomers possess a four-atom-core with atom-to-center distances being less than 2 Å. Both Au_{36-18}^- and Au_{37-16}^- have similar atom-to-center distance distributions and, in particular, have two atoms with their distances to the center longer than 5.5 Å,

confirming the presence of two vertexes on their surfaces. Au_{37-9}^- has three vertexes (whose distances from the center are greater than 5.5 Å) on the surface. When the cluster grows to Au_{38-1}^- , four vertexes arise on the surface, and the cluster has a four-atom tetrahedral core. Au_{38-3}^- also has a four-atom core and four vertexes on the surface. However, the overall shape of Au_{38-3}^- is not as round as Au_{38-1}^- due to having two less vertexes than Au_{38-1}^- in the >5.5 Å area.

Figure 5 demonstrates the structural evolution of the core–shell clusters from Au_{36}^- to Au_{38}^- . Because their structures are

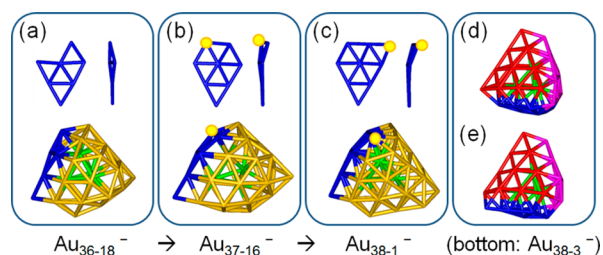


Figure 5. Fragment growth pattern of Au_{36}^- to Au_{38}^- . (a)–(c) Au_{36}^- – Au_{38}^- structural evolution. (d) Au_{38-1}^- (top) and (e) Au_{38-3}^- (bottom). The core Au atoms are highlighted in green. The added atoms from (a) to (c) are highlighted by a yellow sphere.

very similar to one another, the structure of Au_{38-1}^- can be viewed as simply adding one atom on the surface of Au_{37-16}^- or two atoms on Au_{36-18}^- . The added atoms not only change the connected surface and core atoms, but also affect other atoms through Au–Au bond reorganizations. Overall, the cluster's surface becomes smoother and its shape more tetrahedral going from Au_{36}^- to Au_{38}^- . In particular for Au_{38-1}^- , positions of the four vertexes correspond well to its tetrahedral core in space.

The most favorable site for atom additions appears to be the one that makes a more completed triangular Au_{10}^- (with D_{3h} symmetry). The triangular Au_{10}^- is the most stable structure of Au_{10} ,^{15,34} and constitutes the four surfaces of the pyramidal Au_{20} .^{16a} Notably, if we highlight each part of the surface of Au_{38-1}^- and Au_{38-3}^- in different colors (see d, e), we find that the combination of atoms in red and green (core) is analogous to the well-known pyramidal Au_{20}^- (a fragment of FCC bulk gold),^{16a} while the remaining atoms in purple and blue can be viewed as two Au_{10}^- fragments attached to the pyramidal Au_{20}^- . This finding leads to an important conclusion that the Au_{20}^- pyramid is a favorable intermediate in the structural growth toward large-sized Au clusters. One can even imagine bigger clusters being built by packing several Au_{20} clusters together, as suggested in a recent work by Chen and Ren using BH search based on a multiple-center Lennard-Jones potential.³⁵ The special packing in Au_{38} can be viewed as a result of the structural competition between 3D pyramid Au_{20}^- and 2D triangle Au_{10}^- . Because the pyramidal Au_{20} is a fragment of the FCC bulk, we may consider Au_{38} as the beginning of the cluster-to-bulk transformation in gold.

V. CONCLUSION

Through a joint experimental and theoretical study, we find that the most stable structures of Au_{36}^- to Au_{38}^- exhibit the core–shell type structures with a tetrahedral four-atom core. All Au_{36}^- to Au_{38}^- clusters possess two coexisting isomers in the cluster beam. More importantly, a clear growth path from Au_{33}^- to Au_{38}^- through adding Au atoms one-by-one on the surface can be seen. This structural evolution also demonstrates the

tetrahedral four-atom core is highly robust. Last, we find that the structure of Au_{38}^- reflects the interplay between the 3D compact pyramidal structure Au_{20}^- and the 2D compact triangular structure Au_{10}^- . Au_{38-1}^- can be viewed as an Au_{20}^- attached with two incomplete Au_{10}^- , where the four vertices on the surface can better support the tetrahedral core. The appearance of the fragment of FCC bulk gold, that is, pyramidal Au_{20}^- , at Au_{38}^- implies that the cluster-to-bulk transformation is likely to start at Au_{38}^- . In other words, the pyramidal-like intermediates will emerge in later medium- to large-sized Au clusters.

■ ASSOCIATED CONTENT

Supporting Information

Structures of all candidate isomers of Au_{36}^- to Au_{38}^- , and comparison of experimental and theoretical PES spectrum of Au_{37-1}^- . This material is available free of charge via the Internet at <http://pubs.acs.org>.

■ AUTHOR INFORMATION

Corresponding Authors

*E-mail: lai-sheng_wang@brown.edu.

*E-mail: qinwu@bnl.gov.

*E-mail: xzeng1@unl.edu.

Notes

The authors declare no competing financial interest.

■ ACKNOWLEDGMENTS

The experimental work was supported by the National Science Foundation (CHE-1049717 to L.S.W.). X.C.Z. is supported by grants from ARL (W911NF1020099) and the Nebraska Research Initiative. All NWChem and some ADF calculations were performed on the computer clusters at the Center for Functional Nanomaterials, Brookhaven National Laboratory, which is supported by the U.S. Department of Energy, Office of Basic Energy Sciences, under Contract No. DE-AC02-98CH10886. DMol³ calculations were done at the University of Nebraska Holland Computing Center.

■ REFERENCES

- (1) Pyykko, P. Relativistic effects in structural chemistry. *Chem. Rev.* **1988**, *88*, 563–594.
- (2) Hutchings, G. J.; Brust, M.; Schmidbauer, H. Gold - an introductory perspective. *Chem. Soc. Rev.* **2008**, *37*, 1759–1765.
- (3) Wallace, W. T.; Whetten, R. L. Co-adsorption of CO and O₂ on selected gold clusters: Evidence for efficient room-temperature CO₂ generation. *J. Am. Chem. Soc.* **2002**, *124*, 7499–7505.
- (4) Haruta, M. Size- and support-dependency in the catalysis of gold. *Catal. Today* **1997**, *36*, 153–166.
- (5) Chen, M. S.; Goodman, D. W. Catalytically active gold: From nanoparticles to ultrathin films. *Acc. Chem. Res.* **2006**, *39*, 739–746.
- (6) Haruta, M.; Kobayashi, T.; Sano, H.; Yamada, N. Novel gold catalysts for the oxidation of carbon-monoxide at a temperature far below 0° C. *Chem. Lett.* **1987**, *2*, 405–408.
- (7) Yoon, B.; Hakkinen, H.; Landman, U.; Worz, A. S.; Antonietti, J. M.; Abbet, S.; Judai, K.; Heiz, U. Charging effects on bonding and catalyzed oxidation of CO on Au₈ clusters on MgO. *Science* **2005**, *307*, 403–407.
- (8) Green, I. X.; Tang, W. J.; Neurock, M.; Yates, J. T. Spectroscopic observation of dual catalytic sites during oxidation of CO on a Au/TiO₂ catalyst. *Science* **2011**, *333*, 736–739.
- (9) Li, L. G. Y.; Li, H.; Zhao, Y.; Pei, Y.; Chen, Z. F.; Zeng, X. C. CO oxidation on TiO₂ (110) supported subnanometer gold clusters: Size and shape effects. *J. Am. Chem. Soc.* **2013**, *135*, 19336–19346.
- (10) Lopez, N.; Norskov, J. K. Catalytic CO oxidation by a gold nanoparticle: A density functional study. *J. Am. Chem. Soc.* **2002**, *124*, 11262–11263.
- (11) Lemire, C.; Meyer, R.; Shaikhtudinov, S.; Freund, H. J. Do quantum size effects control CO adsorption on gold nanoparticles? *Angew. Chem., Int. Ed.* **2004**, *43*, 118–121.
- (12) Liu, C. Y.; Tan, Y. Z.; Lin, S. S.; Li, H.; Wu, X. J.; Li, L.; Pei, Y.; Zeng, X. C. CO self-promoting oxidation on nanosized gold clusters: Triangular Au₃ active site and CO induced O-O scission. *J. Am. Chem. Soc.* **2013**, *135*, 2583–2595.
- (13) Xing, X. P.; Yoon, B.; Landman, U.; Parks, J. H. Structural evolution of Au nanoclusters: From planar to cage to tubular motifs. *Phys. Rev. B* **2006**, *74*, 165423.
- (14) Lechtken, A.; Neiss, C.; Kappes, M. M.; Schooss, D. Structure determination of gold clusters by trapped ion electron diffraction: Au₁₄⁻–Au₁₉⁻. *Phys. Chem. Chem. Phys.* **2009**, *11*, 4344–4350.
- (15) Hakkinen, H.; Yoon, B.; Landman, U.; Li, X.; Zhai, H. J.; Wang, L. S. On the electronic and atomic structures of small Au_N⁻ (N=4–14) clusters: A photoelectron spectroscopy and density-functional study. *J. Phys. Chem. A* **2003**, *107*, 6168–6175.
- (16) (a) Li, J.; Li, X.; Zhai, H. J.; Wang, L. S. Au₂₀: A tetrahedral cluster. *Science* **2003**, *299*, 864–867. (b) Bulusu, S.; Li, X.; Wang, L. S.; Zeng, X. C. Evidence of hollow golden cages. *Proc. Natl. Acad. Sci. U.S.A.* **2006**, *103*, 8326–8330.
- (17) (a) Johansson, M. P.; Lechtken, A.; Schooss, D.; Kappes, M. M.; Furche, F. 2D-3D transition of gold cluster anions resolved. *Phys. Rev. A* **2008**, *77*, 053202. (b) Huang, W.; Wang, L. S. Probing the 2D to 3D structural transition in gold cluster anions using argon tagging. *Phys. Rev. Lett.* **2009**, *102*, 153401.
- (18) Bulusu, S.; Li, X.; Wang, L. S.; Zeng, X. C. Structural transitions from pyramidal to fused planar to tubular to core/shell compact in gold clusters: Au_n⁻ (n=21–25). *J. Phys. Chem. C* **2007**, *111*, 4190–4198.
- (19) Shao, N.; Huang, W.; Gao, Y.; Wang, L. M.; Li, X.; Wang, L. S.; Zeng, X. C. Probing the structural evolution of medium-sized gold clusters: Au_n⁻ (n = 27–35). *J. Am. Chem. Soc.* **2010**, *132*, 6596–6605.
- (20) Gu, X.; Bulusu, S.; Li, X.; Zeng, X. C.; Li, J.; Gong, X. G.; Wang, L. S. Au₃₄: A fluxional core-shell cluster. *J. Phys. Chem. C* **2007**, *111*, 8228–8232.
- (21) Ji, M.; Gu, X.; Li, X.; Gong, X. G.; Li, J.; Wang, L. S. Experimental and theoretical investigation of the electronic and geometric structures of the Au₃₂ cluster. *Angew. Chem., Int. Ed.* **2005**, *44*, 7119–7123.
- (22) (a) Lechtken, A.; Schooss, D.; Stairs, J. R.; Blom, M. N.; Furche, F.; Morgner, N.; Kostko, O.; von Issendorff, B.; Kappes, M. M. Au₃₄⁻: A chiral gold cluster? *Angew. Chem., Int. Ed.* **2007**, *46*, 2944–2948. (b) Jiang, D. E.; Walter, M. Au₄₀: A large tetrahedral magic cluster. *Phys. Rev. B* **2011**, *84*, 193042.
- (23) Huang, W.; Ji, M.; Dong, C. D.; Gu, X.; Wang, L. M.; Gong, X. G.; Wang, L. S. Relativistic effects and the unique low-symmetry structures of gold nanoclusters. *ACS Nano* **2008**, *2*, 897–904.
- (24) Zhao, L. X.; Zhang, M.; Feng, X. J.; Zhang, H. Y.; Zhang, W. L.; Luo, Y. H. Stuffed cage structures and properties of neutral and charged Au₃₈ nanocluster. *J. Cluster Sci.* **2013**, *24*, 123–131.
- (25) Wales, D. J.; Scheraga, H. A. Review: Chemistry - Global optimization of clusters, crystals, and biomolecules. *Science* **1999**, *285*, 1368–1372.
- (26) Huang, W.; Bulusu, S.; Pal, R.; Zeng, X. C.; Wang, L. S. CO chemisorption on the surfaces of the golden cages. *J. Chem. Phys.* **2009**, *131*, 234305.
- (27) Wang, L. S.; Cheng, H. S.; Fan, J. W. Photoelectron spectroscopy of size-selected transition-metal clusters - Fe_N⁻, n = 3–24. *J. Chem. Phys.* **1995**, *102*, 9480–9493.
- (28) Wang, L. M.; Wang, L. S. Probing the electronic properties and structural evolution of anionic gold clusters in the gas phase. *Nanoscale* **2012**, *4*, 4038–4053.
- (29) Perdew, J. P.; Burke, K.; Ernzerhof, M. Generalized gradient approximation made simple. *Phys. Rev. Lett.* **1996**, *77*, 3865–3868.

(30) Delley, B. An all-electron numerical-method for solving the local density functional for polyatomic-molecules. *J. Chem. Phys.* **1990**, *92*, 508–517.

(31) Delley, B. From molecules to solids with the DMol³ approach. *J. Chem. Phys.* **2000**, *113*, 7756–7764.

(32) ADF 2013; SCM, Theoretical Chemistry, Vrije Universiteit: Amsterdam, The Netherlands (<http://www.scm.com>).

(33) Valiev, M.; Bylaska, E. J.; Govind, N.; Kowalski, K.; Straatsma, T. P.; Van Dam, H. J. J.; Wang, D.; Nieplocha, J.; Apra, E.; Windus, T. L.; de Jong, W. NWChem: A comprehensive and scalable open-source solution for large scale molecular simulations. *Comput. Phys. Commun.* **2010**, *181*, 1477–1489.

(34) Huang, W.; Wang, L. S. Au₁₀⁻: isomerism and structure-dependent O₂ reactivity. *Phys. Chem. Chem. Phys.* **2009**, *11*, 2663–2667.

(35) Ren, L.; Cheng, L. J. Structural prediction of (Au₂₀)_N (N=2–40) clusters and their building-up principle. *Comput. Theor. Chem.* **2012**, *984*, 142–147.